

*Article*

## Effects of Weave Pattern on Filtration Performance of Woven Filter Cloths by Computational Fluid Dynamic Modeling

Wisit Bandasak<sup>1,a</sup> and Pimporn Ponpesh<sup>1,2,b,\*</sup>

<sup>1</sup> Department of Chemical Engineering, Faculty of Engineering, Chulalongkorn University, Bangkok 10330, Thailand

<sup>2</sup> Control Research Unit, Faculty of Engineering, Chulalongkorn University, Bangkok 10330, Thailand

E-mail: <sup>a</sup>Wisit124@gmail.com, <sup>b,\*</sup>pimporn.p@chula.ac.th (Corresponding author)

**Abstract.** Outdoor physical activities are essential for maintaining a healthy lifestyle, but they can also expose individuals to harmful air pollutants such as particulate matter. Particulate matter, especially those with a diameter of less than 10  $\mu\text{m}$  ( $\text{PM}_{10}$ ), can penetrate deep into the lungs and cause adverse health effects such as respiratory diseases, cardiovascular diseases, and even premature deaths. Consequently, masks are essential while outside with high PM pollution. Additionally, the COVID-19 pandemic has made it necessary for people to wear masks as a protective measure against the virus while engaging in outdoor activities. However, not all masks provide adequate protection against both the virus and particulate matters. This study aimed to investigate the effect of weave patterns on the filtration performance of woven filter cloths using Computational Fluid Dynamics (CFD) simulations. A laminar-flow model was applied due to low Reynolds number of the face velocity. Specifically, the study focused on  $\text{PM}_{10}$ . The filtration process was examined in a relation to three weave patterns: plain weave, twill weave, and satin weave, using the CFD model. The Discrete Phase Model (DPM) was used for simulating the particulate matter trajectories. The numerical model was validated with the data from Konda et al (2020) [19]. The results showed that the twill and satin weaves had higher filtration efficiencies than the plain weave. Finally, the findings of this study will be used to guide the manufacturing of masks that are suitable for protecting individuals from the dust and viruses while exercising.

**Keywords:** CFD, weave pattern, filtration efficiency, filter cloths, masks, aerosols.

ENGINEERING JOURNAL Volume 28 Issue 1

Received 23 June 2023

Accepted 11 January 2024

Published 31 January 2024

Online at <https://engj.org/>

DOI:10.4186/ej.2024.28.1.23

## 1. Introduction

Air pollution is an environmental problem that directly affects the respiratory system and health of all living organisms, humans including [1]. This can occur naturally or may be caused by humans, such as roadside pollution, open burning, factory pollution, agricultural activities, and some types of gas emissions. The most concerned pollutants at present are PM<sub>2.5</sub> and PM<sub>10</sub> (PM with an aerodynamic diameter of 2.5 μm or less and 10 μm or less, respectively), which are increased significantly from the past [2], making it necessary for people to wear masks that can filter these particulate matters when being exposed in a polluted environment.

Since year 2019 the COVID-19 disease has caused global infections, illnesses, and deaths, and had a significant impact on daily life. In addition to the spread of particulate matter, it is now believed that the SARS-CoV-2 virus can also spread through inhaled aerosols [3]. The Centers for Disease Control and Prevention (CDC) recommend wearing a respiratory mask or face covering in public places and practicing social distancing to prevent the spread of the virus [4]. Therefore, it is necessary to wear a mask when in a risky environment, even while exercising, to prevent the infection. While N95 or other equivalent masks are recommended, they tend to be less comfortable and can make it difficult to breathe during exercises [5, 6]. Thus, cloth masks have been considered as a substitute for exercising.

Cloths come in various weaving styles which is a repeated pattern of the basic designs. The common weaving styles are Plain, Twill, and Satin, but each style can be further subdivided. Each style provides different size gaps and has different efficiency in filtering, which affects the strength, flexibility, and beauty of the fabric [7]. Additionally, the type of fabric also affects its filtering ability, such as Cotton, Chiffon, or Silk, which are woven from different thread densities. Moreover, there are non-woven fabrics that can be made from polymers without weaving or knitting. Tung et al. (2002) [8] reported that satin weave fabrics allow for more efficient fluid flow compared to plain weave fabrics under the same thread count. The research conducted by S.I. Green (2008) [9] suggested that changing the position of fibers affects the fluid behavior and pressure drop across the fabric. Studies have been conducted to analyze the filtration efficiency of individual fibers using ANSYS CFD [10], Lattice-Boltzmann method, or Discrete Element Method (DEM) [11]. However, these studies were conducted based on individual fibers which cannot fully represent the actual filtration efficiency of real fibers. Therefore, recent studies have focused on using real fibers to mimic the filtration process. Real fibers are classified into three categories based on their structure: unidirectional, 3-Dimension random, and layered [12].

There are five mechanisms in the filtration of aerosol in sub-micron size fibrous media: inertial impaction, gravity, direct interception, diffusion, and electrostatic interaction [13, 14]. When dealing with aerosols ranging

from approximately 1 μm to 10 μm in diameter, both direct interception and inertial impaction [15] are the significant mechanisms. Direct interception happens when the particles encounter filter fibers and get stuck due to their size and shape. On the other hand, inertial impaction occurs when larger particles cannot follow the path of the gas streamlines and instead collide with filter fibers due to their momentum. And lastly, diffusion filtration is effective for capturing particles smaller than 0.1 μm in diameter due to their susceptibility to Brownian motion and lower inertia [16]. Each filtration method is suitable for different particle sizes, types, and masses, and their efficiencies often overlap, leading to varying levels of retention efficiency. The filtration mechanism with the lowest efficiency is Brownian diffusion filtration, which is the most effective for smaller particles. In contrast, inertial impaction and interception filtration become dominant at higher particle sizes and exhibit the highest penetration for particles of a specific size range. The Most Penetrating Particle Size (MPPS) varies depending on the filter type [17]. Brownian diffusion is known to be dominant when the particle size is very small and obtaining filtering efficiency is difficult. As a result, this simulation attempts to predict the performance of filter cloth with particle sizes ranging from 30 nm to 10 μm.

The objective of this research is to investigate the effects of weave patterns on the filtration performance of woven filter cloths using the CFD simulations by Ansys Fluent software (Ansys Inc., Pennsylvania, United States). The Laminar model was used due to the low Reynolds number of the face velocity. It is also aimed to determine the most efficient weaving pattern for cloth masks suitable for exercise.

## 2. Methodology

### 2.1. Model Geometry

The model geometry of the fibers was created according to Peirce's mathematical model as shown in Fig. 1 [18]. Peirce's model was utilized to determine the parameters for the geometrical structure of a plain weave fabric with circular threads. The mathematical equations which relate the fabric structural parameters in Peirce's model are as follows [18, 19]:

$$h_j + h_w = D_j + D_w = D \quad (1)$$

$$\frac{h_j}{\alpha_w} = \frac{4}{3} \sqrt{c_j}; \quad \frac{h_w}{\alpha_j} = \frac{4}{3} \sqrt{c_w} \quad (2)$$

$$\alpha_w = (l_j - D\theta_j) \cos\theta_j + D \sin\theta_j \quad (3)$$

$$\alpha_j = (l_w - D\theta_w) \cos\theta_w + D \sin\theta_w \quad (4)$$

$$c_j = \frac{l_j}{A} - 1 = \frac{l_j}{\alpha_w} - 1; \quad c_w = \frac{l_w}{B} - 1 = \frac{l_w}{\alpha_j} - 1 \quad (5)$$

$$l_j = \frac{L_j}{N_w}; \quad l_w = \frac{L_w}{N_j} \quad (6)$$

$$\alpha_w = \frac{A}{N_j} = \frac{l_j}{1+c_j} = \frac{L_j}{N_w} \frac{1}{1+c_j} \quad (7)$$

$$\alpha_j = \frac{B}{N_w} = \frac{l_w}{1+c_w} = \frac{L_w}{N_j} \frac{1}{1+c_w} \quad (8)$$

where  $D_j$  and  $D_w$  are the diameters of warp and weft;  $\alpha_w$  and  $\alpha_j$  are the spacing between the adjacent weft or warp;  $c_j$  and  $c_w$  are the warp and weft shrinkage of fabric;  $h_j$  and  $h_w$  are the crimp wave heights of warp or weft;  $l_j$  and  $l_w$  are the crimp wave lengths of warp or weft;  $L_j$  and  $L_w$  are the lengths of warp or weft;  $N_j$  and  $N_w$  are the numbers of warp or weft;  $\theta_j$  and  $\theta_w$  are the contact angles of warp cover on weft or weft cover on warp;  $A$  is the length of the fabric; and  $B$  is the width of the fabric.

However, some geometrical shapes such as tangential connection and partial overlap were modified to improve the mesh quality. Thus, the above model was slightly adjusted. The computational domain was generated to represent the fabrics area of 4.5mm x 4.5mm which covered the smallest repeating pattern of the fabrics in this study. In addition, 80 and 300 threads per inch (TPI) woven fabrics were simulated for model validation [20] and further analysis. The fibers' warp and weft diameters were both 0.27 mm. The distance between the warp cover and the weft is 0.27 mm and the contact angle is about 29.21 degrees. The model is shown in Fig. 2.

## 2.2. Computational Domain and Meshes

To prevent any objects or surfaces from obstructing or disrupting the smooth and continuous movement of the fluid, the inlet and outlet were separated from the fibers approximately 10 times the diameter of the fiber [21]. Thus, the flow field was assumed to have no effects on the inlet and outlet calculation zones. The dimension of the computational domain was 4.5 mm x 4.5 mm x 6.12 mm as shown in Fig. 3. In addition, the meshes were composed of 3.4 million tetrahedral elements, with an overall element size of 0.08 mm. However, the meshes in the body of influence were slightly finer to capture the gradients that occurred in the fiber zone. This helped reduce the element size and improve the mesh quality for the curves and the overlapping parts. The average value of the skewness was 0.21. The meshed geometry is shown in Fig. 4.

## 2.3. Governing Equations

The required governing equations included the conservations of mass and momentum (temperature gradient neglected). Based on Reynolds number calculation, the flow regime was laminar. Thus, Navier-Stokes equation was applied for momentum conservation. It can be written as follows:

$$\rho \frac{D\vec{u}}{Dt} + \nabla p = \mu \nabla^2 \vec{u} + \rho \vec{g} + \vec{S}_{add} \quad (9)$$

where  $p$  is the static pressure,  $\rho$  is the fluid density,  $\vec{u}$  is the fluid velocity,  $\mu$  is the dynamic viscosity and  $\vec{g}$  is the gravitational acceleration and  $\vec{S}_{add}$  is for additional source terms.

In addition, to simulate the gas-solid two-phase flow the Discrete Phase Model (DPM), which applies the Euler-Lagrange approach [22, 23], was used. The DPM tracks particles in a continuous flow regime. The particles are considered as separate entities that move through the fluid by following the fluid velocity field in this technique. In addition, the model is suitable for a situation in which the particle volume fraction is so small relative to the fluid volume, such that the presence of the particles has no major effect on the flow field [24]. The trajectory of particles is governed by Newton's second law of motion, which includes drag and buoyancy forces. In this study, for sub-micron particles additional forces such as Brownian and Saffman's lift force were integrated. The force-balance equation for the particle flow can be expressed as follows:

$$\frac{\partial \vec{u}_p}{\partial t} = F_D (\vec{u} - \vec{u}_p) + \frac{\vec{g}(\rho_p - \rho)}{\rho_p} + \vec{F}_i \quad (10)$$

where  $\vec{u}_p$  is the particle velocity,  $\rho_p$  is the particle density which was considered as the density of sodium chloride (i.e., 2170 kg/m<sup>3</sup>),  $\vec{F}_i$  is additional acceleration terms. The expression of  $F_D$  or drag force is as follows:

$$F_D = \frac{18\mu}{\rho_p d_p^2 C_C} \quad (11)$$

$$C_C = 1 + K_{np} (1.257 + 0.4e^{-1.1/K_{np}}) \quad (12)$$

where  $d_p$  is the particle diameter,  $C_C$  is the Cunningham correction factor [25],  $K_{np} = \lambda/d_p$  is the Knudsen number, and  $\lambda$  is mean free path of the fluid molecule. For the submicron particles with very low Reynolds number, Saffman's lift force ( $F_S$ ) was included [26]. The expression of  $F_S$  is as follows:

$$F_S = \frac{2Kv^{1/2}\rho d_{ij}}{\rho_p d_p (d_{ik}d_{kl})^{1/4}} (\vec{u} - \vec{u}_p) \quad (13)$$

where  $K = 2.594$ ,  $\nu$  is the kinematic viscosity of fluid, and  $d_{ij}$  is the deformation tensor. Furthermore, Brownian force ( $F_B$ ) was also considered for the small particles. However, when the velocity is increased the effect of Brownian force may decrease. The expression of  $F_B$  is as follows:

$$F_B = \xi \sqrt{\frac{216\mu k_B T}{\pi \rho_p^2 d_p^5 C_C \Delta t}} \quad (14)$$

where  $\xi$  represents a random number from the standard normal distribution,  $k_B$  is the Boltzmann constant,  $T$  is thermodynamic temperature, and  $\Delta t$  is time step.

For micron particles, the Spherical law of drag force was used, and the impact of gravity was considered [27]. The expression of the drag force is as follows:

$$F_D = \frac{3\eta C_D Re}{4\rho_p d_p^2} \quad (15)$$

$$\overline{Re} = \frac{\rho_d |\vec{u}_p - \vec{u}|}{\mu} \quad (16)$$

$$C_D = \frac{24}{Re} \quad (Re \leq 0.1) \quad (17)$$

$$C_D = 3.69 + 22.73\sqrt{Re} + 0.0903\sqrt{Re^2} \quad (0.1 \leq Re \leq 1) \quad (18)$$

where  $Re$  is the Reynolds number,  $\overline{Re}$  is the relative Reynolds number, and  $C_D$  is the drag coefficient. For the relative Reynolds number of less than 0.1, the drag coefficient  $C_D$  of  $24/Re$  and the Stokes Cunningham drag law were applied. Moreover, when the relative Reynolds number is between 0.1 and 1, the spherical drag law provides a more precise description of the drag coefficient  $C_D$ .

## 2.4. Boundary Condition

This simulation was performed in steady state with the Laminar flow model using Ansys Fluent software. The boundary conditions for the inlet and outlet were set to 'velocity inlet' and 'pressure outlet' respectively. The inlet and outlet boundary conditions for the DPM were set to 'escape'. In addition, the surfaces of the fibers were specified as 'trap' condition. This was to account for particle deposition onto the filter fibers. The inlet and outlet were positioned away from the fibers at a distance of 10 times the fiber diameter to avoid disturbing the fluid flow. As a result, the fluid may be assumed to be completely developed in the control domain, and the particles to be in an undisturbed flow field. In the study of Konda et al (2020) [20], the researchers evaluated the

filtration efficiency of commonly available fabrics used in cloth masks. Sodium chloride aerosol particles were employed to replicate respiratory droplets and aerosols [20]. They utilized an aerosolized NaCl solution to generate particles in two size ranges: less than 300 nm and greater than 300 nm. The size dimensions and concentrations were measured using specialized particle sizers. NaCl aerosol particles were also used in this study.

The Discrete phase model was used in this study to simulate the transport of NaCl aerosols. Surface injection was used to introduce the particles to the control domain by specifying the mass flow rate. The particle distribution was estimated from the study done by Konda et al (2020) [19]. All particles were inert, and the total mass flow rate of NaCl aerosols was computed from ultrafine particles ranging in sizes from 6 to 220 nm recorded near a major highway [28]. To achieve the filtering mechanism, the Saffman's lift force and Brownian motion function were activated in the DPM. Moreover, the buoyancy force was applied when the gravity force was enabled. The outlet was set as pressure-outlet condition which equals to the atmospheric pressure. Additionally, the simulated fibers were only a portion of the filter cloth; and there was no substantial lateral airflow present. Consequently, the symmetry boundary condition was applied to the walls of the computational domain [29]. Since Knudsen number was very low, thus the flow was the stoke flow.

When the intensity of the activity increases, so does the rate of breathing. The lowest and maximum breathing flow rates are 6 and 85 litres per minute (LPM), respectively [30]. In this study, the flow velocity was estimated for the typical mask area of 190 cm<sup>2</sup> [31]. The values ranged from 0.5 to 7.5 cm/s for 6 and 85 LPM breathing flow rates, respectively.

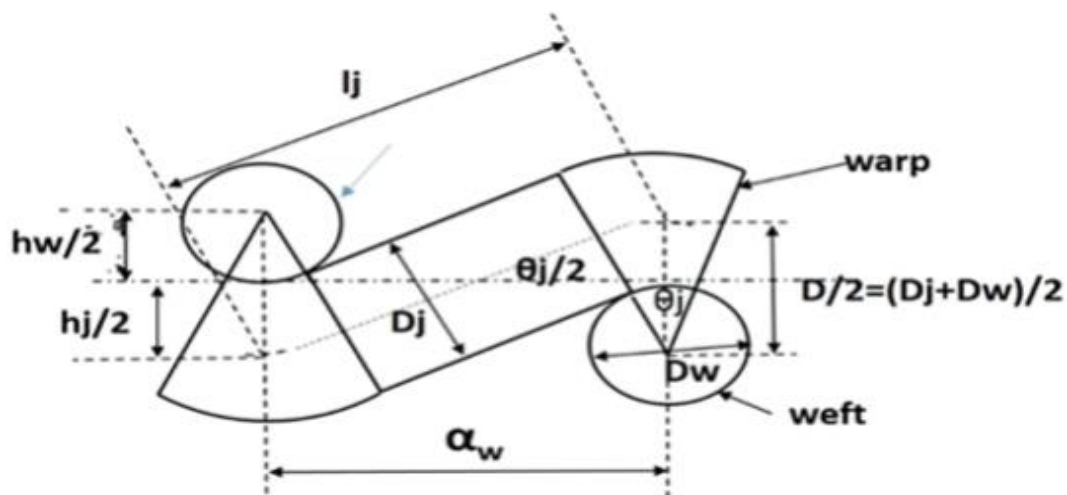


Fig. 1. Peirce geometric model of woven fabric [19].

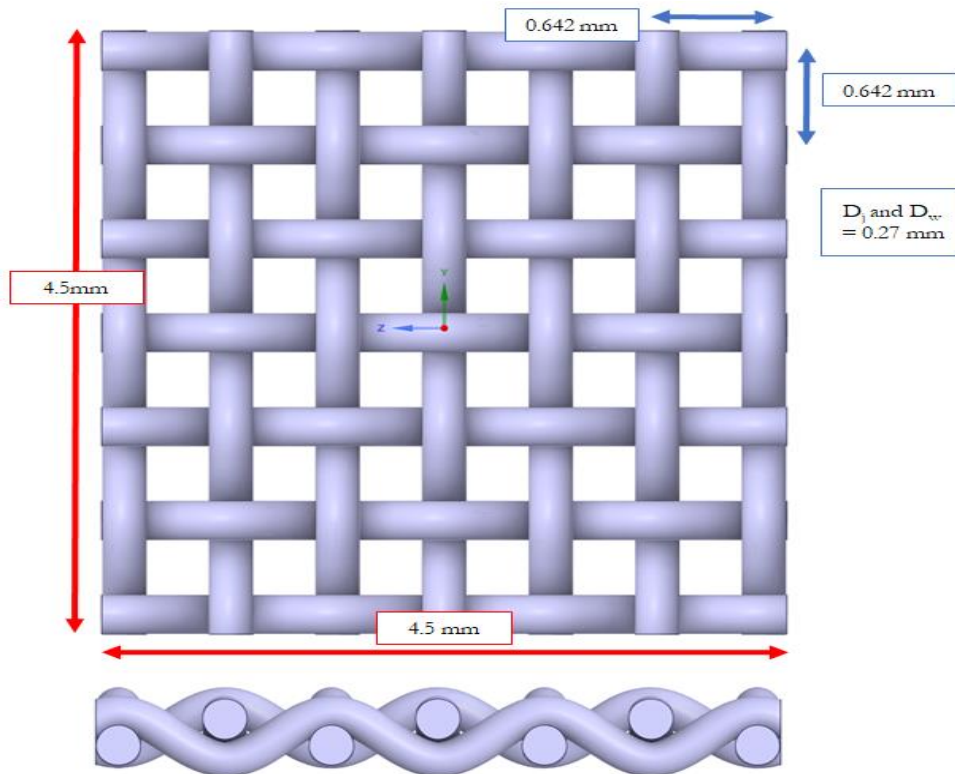


Fig. 2. The geometry of the fibers model of which the weft and warp have equal diameters, i.e., 0.27 mm, to resemble quilter's cotton with a thread count of 80 threads per inch.

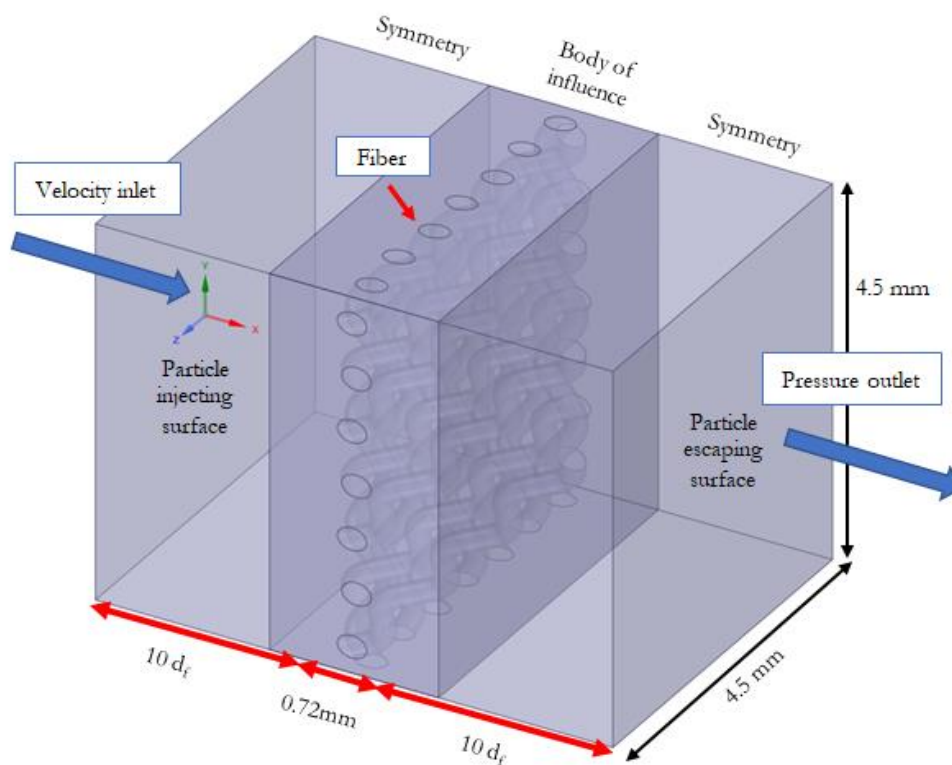


Fig. 3. Simulation domain and boundary conditions (solid-volume-fraction of fibers to the simulation domain of about 0.27 and fiber diameter ( $d_f$ ) of 270  $\mu\text{m}$ ).

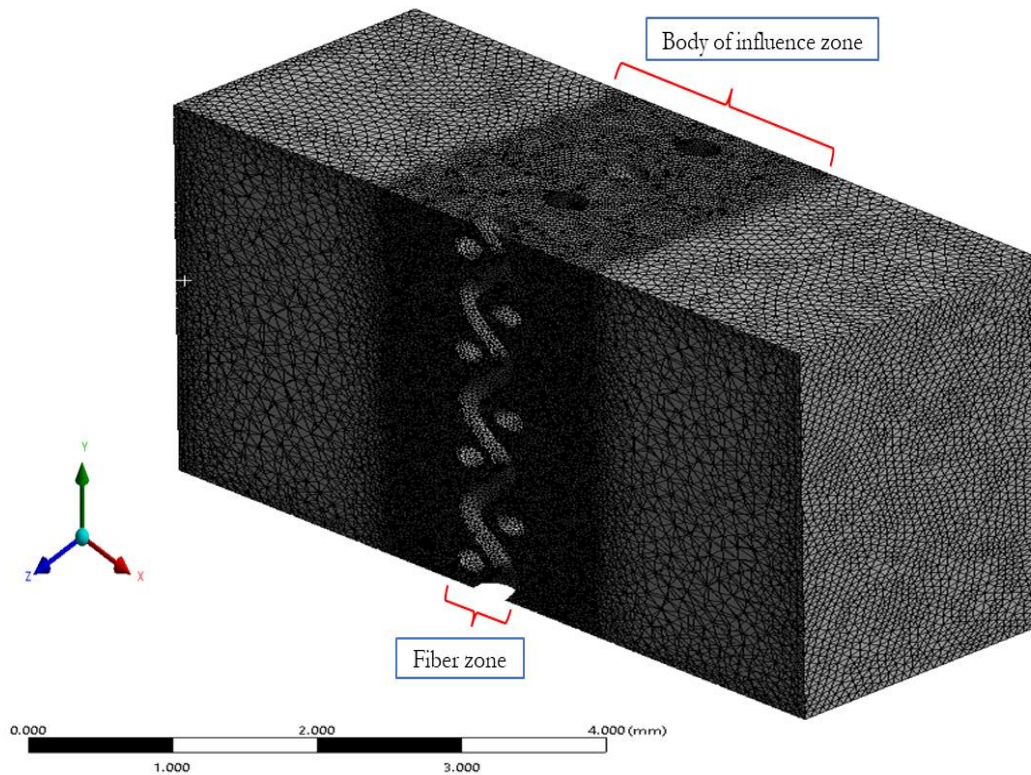


Fig. 4. The meshed geometry with an overall element size of 0.08 mm and a slightly finer mesh of 0.05 mm in the body of influence zone.

## 2.5. Investigation of Weave-Pattern Effects on the Filtration Performance

Three basic weave patterns of filter cloths were studied. These include plain, twill, and satin weave. When there are changes in the interlacing or weaving pattern of fibers, they can have an impact on the airflow passing through the filter fabric. A modification to the weave pattern can lead to corresponding changes in the airflow characteristics as it moves through the fabric. Consequently, the movement of particles through the air is also affected, resulting in different filtration efficiencies. This study neglected the change in fiber size caused by particle deposition on the fibers. Despite the distinct patterns of satin, twill, and plain weave, to adequately compare the effects of weave pattern it is essential to maintain the same fiber diameter (i.e., 0.27 mm), contact angle (i.e., 29.21 degrees), and thread count (i.e., 80 or 300 TPI).

## 3. Results and Discussion

### 3.1. Model Validation

#### Pressure drop

Pressure drop of the fibrous media is an important factor. The flow of air through the fibrous media is laminar. The expression of pressure drop follows the Darcy-Forchheimer equation which has been extensively

used in literature to explain the pressure drop of fibrous media. It can be written as follows [32]:

$$\frac{\Delta p}{L} = f(\alpha) \frac{\mu v}{d_f^2} \quad (19)$$

where  $L$  is the filter medium thickness,  $f(\alpha)$  is the dimensionless drag coefficient as a function of solid-volume-fraction (SVF),  $\alpha$  is the solid volume fraction of fibrous media,  $v$  is filtration velocity, and  $d_f$  is the fiber diameter. Many formulas for  $f(\alpha)$  based on different theories exist, for example: the formulas from Happel (1959) [33], Kuwabara (1959) [34], and others. The expression from the study of Happel (1959) is simply defined as follows:

$$f(\alpha) = \frac{16\alpha}{-0.5 \ln \alpha - 0.5 \frac{1-\alpha^2}{1+\alpha^2}} \quad (20)$$

The expression from the study by Kuwabara (1959) was given on the basis that the surface curl of cylinder was zero, more precisely if the horizontal and vertical distances between fibers are equal. The expression from Kuwabara (1959) is as follows:

$$f(\alpha) = \frac{16\alpha}{-0.5 \ln \alpha + \alpha - 0.75 - 0.25\alpha^2} \quad (21)$$

Other two popular expressions were proposed by Davies (1973) [35] and Rao (1988) [36], which were experimental and numerical studies, respectively. Both studies investigated the pressure drop of fibrous medium.

The expressions for Davies' and Rao's models are written in Eq. (22) and (23), respectively.

$$f(\alpha) = 64\alpha^{1.5}(1+56\alpha^3) \quad (22)$$

$$f(\alpha) = 2.653\alpha + 39.34\alpha^2 + 144.5\alpha^3 \quad (23)$$

The comparison of the simulated pressure drops at different filtration velocities for a plain weave model with the values from Happel's and Davies' models is illustrated in Fig. 5. The plain weave model was consisted of 300 TPI with a diameter of 0.065 mm. Equations (1)-(8) were used to create the model. It is shown that the simulated results from this study are in good agreement with the Happel's and Davies' models, which are theoretical and empirical models, respectively. These findings demonstrate that the simulated fiber model can accurately predict the filtering performance of real filter cloths. Overall, these results provide strong validation for the use of this simulation model to explore the impact of different weave patterns on the filtration efficiency of woven filter cloths.

### Filtration efficiency

The filtration efficiency ( $E$ ) of the fibers can be written as follows:

$$E = 1 - \frac{N_{out}}{N_{in}} \quad (24)$$

where  $N_{in}$  and  $N_{out}$  are the total numbers of particles at the inlet and outlet, respectively. The simulation was validated by comparing its results with the data obtained from Konda et al (2020) [20]. The values of filtration efficiency of Quilter's 80 TPI cotton mask at a flow rate of 1.2 cubic feet per minute (CFM) were compared as shown in Fig. 6. In addition, Sodium Chloride (NaCl)

aerosols were employed to create particles of varying sizes, i.e., 28, 37, 49, 65.5, 87.5, 116.5, 155.5 and 450 nm.

In this study, the behaviours of the particles were determined by the forces acting on the particles with different sizes (i.e., drag force, Brownian force, and Saffman lift force). The trajectories of the particles were simulated by DPM. Brownian force was applied to analyse the particle diffusion. Particle deposition was estimated by the 'trap boundary condition' in the DPM which traps the particle and terminates its trajectory after the particle hits the surfaces of the fibers. Figure 6 shows the validation of simulated filtration efficiencies with the results from the experiment by Konda et al (2020) [20]. From this figure, the simulated filtration efficiencies are higher than the experimental data for particles with sizes smaller than about 0.3  $\mu\text{m}$ . It might be explained by the trap boundary condition which over-predict the deposition of these small particles. In addition, this study did not consider the expansion of fiber cross-section and dendrite formation due to particle deposition. These can occur in the experiment and enhance the interception [37] a major mechanism for larger particles (i.e., approximately 1  $\mu\text{m}$  and larger). Moreover, the simplifications to the computational geometry, in which tangential connection and partial overlap were modified to improve the mesh quality, might increase inter-fiber gaps and result in reduced flow velocity through fiber zone, leading to lower inertial impact especially for larger particles. Consequently, the filtration efficiency for larger particles in the experiment is higher compared with the simulation. Furthermore, the micro-structures of fiber materials which were neglected in the simulation can also contribute to the deviation of the simulated results from the experimental data [37]. Finally, despite these limitations, the CFD model can follow the trend and can provide the prediction within the variability of the experimental data.

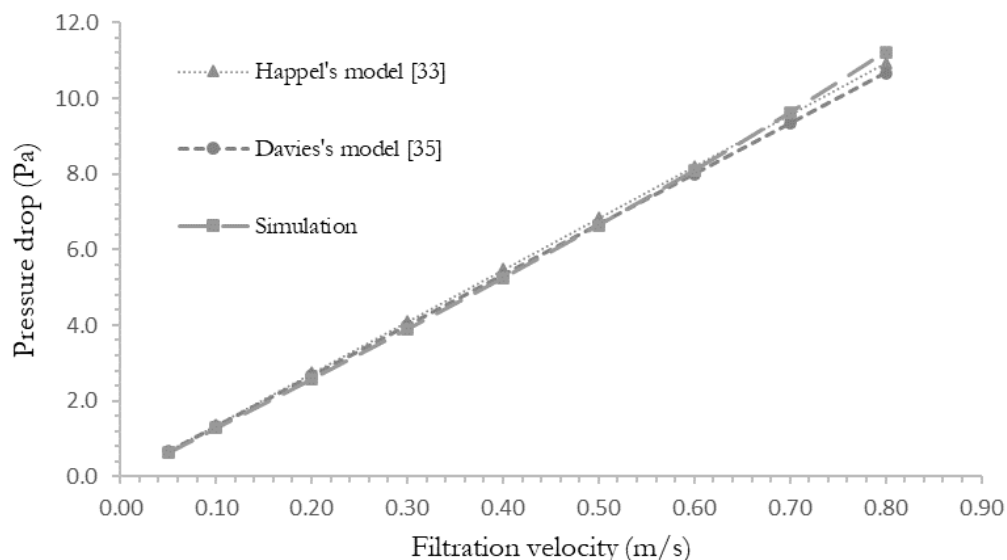


Fig. 5. Comparison of pressure drop from the experimental studies and the simulation (plain weave model with 0.065 mm diameter and 300 TPI).

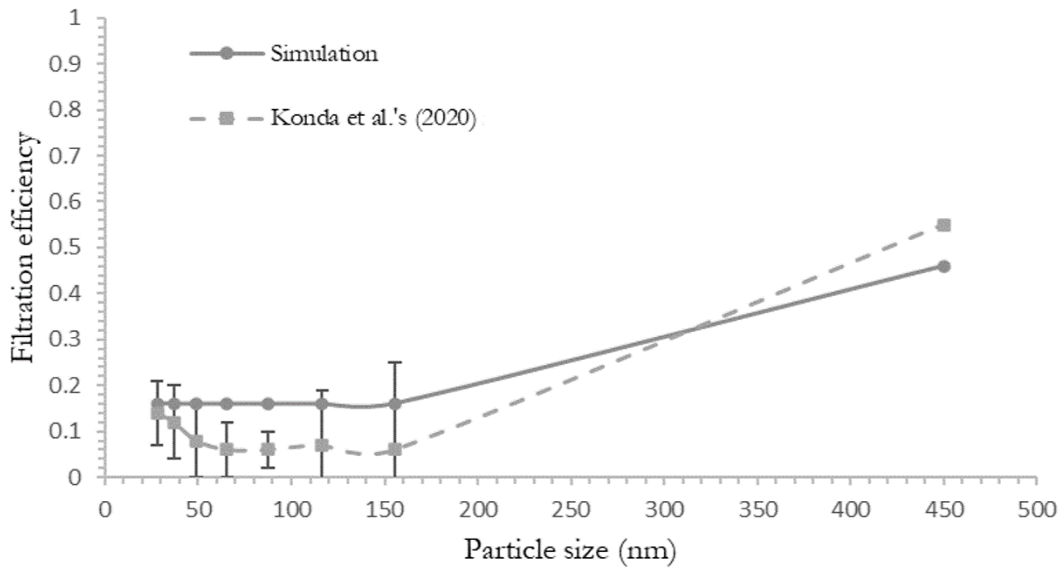


Fig. 6. The filtration efficiencies of cotton plain-weave with 80 TPI and at a flow rate of 1.2 CFM.

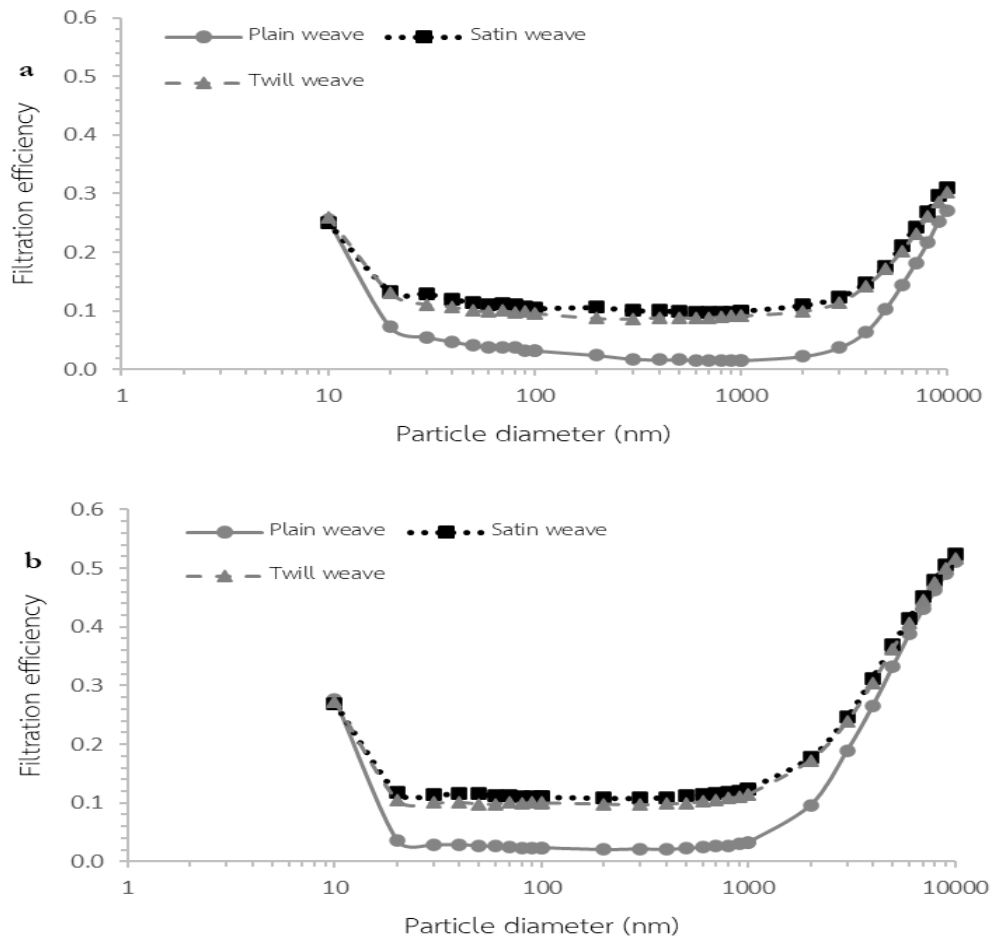


Fig. 7. Filtration efficiency of plain, satin, and twill weaves with 300 threads per inch at varied filtration flow velocities: (a) 0.05 m/s and (b) 0.27 m/s.

### 3.2. Influence of Weave-Pattern

The impact of weave patterns on the filtration performance plays an important role in filtration system optimization. A modification to interlacing of fibers or weave pattern has a direct impact on the flow characteristics and filtration efficiency. This section will discuss the influences of three common weave patterns: plain weave, satin weave, and twill weave, on the filtration efficiency at two different flow velocity, i.e., 0.05 m/s and 0.27 m/s, which represent resting and moderate exertion, respectively [30]. Higher velocities during exertion can lead to increased turbulence in the airflow, potentially causing particles to deviate from their original trajectories and disperse more widely. Resulting in particles that follow the air will also cause different filtration efficiency.

Figure 7 illustrates the filtration efficiencies of different weave patterns, namely plain, satin, and twill at flow velocities of 0.05 m/s (Fig. 7a) and 0.27 m/s (Fig. 7b), all having a thread count of 300 TPI. The results are consistent with the characteristics of the total filter efficiency for particles with different sizes as illustrated by Hinds (1999) [32]. That is, diffusion is the only important mechanism for submicron particles and diminished for larger particles. Interception and inertial impaction are negligible for small particles but become the major mechanisms for larger particles. In addition, all filters have minimum efficiency at the in-between sizes, usually about 0.05 – 0.5  $\mu\text{m}$ , in which particles are too large for diffusion and too small for interception or inertial impaction [32]. The associated particle size ranges can vary depending on the characteristics of filter materials and face velocity.

In addition, Fig. 7 consistently demonstrate that the satin weave exhibits the highest filtration efficiency, followed by the twill weave, while the plain weave consistently performs the least efficiency for both velocities. Interestingly, the filtration efficiencies of the satin and twill weaves show similar results in capturing very small particles in submicron range and larger particle of micron sizes at both tested velocities. This phenomenon is consistent with the study by Cao et al. (2020) [27]. As the particle size becomes smaller (e.g.,  $\leq 10$  nm) in the submicron range, Brownian diffusion has a particularly notable effect on filtration efficiency at both velocities regardless of the weave pattern. It greatly depends on the particle size and fluid properties [38].

### 4. Conclusion

This study was aimed at investigating the impact of weave patterns on the filtration performance of woven filter cloths. The Computational Fluid Dynamics model was developed and validated with the values of pressure drop and filtration efficiency from empirical and theoretical models, as well as experimental measurements [20, 33, 35]. From the comparison of pressure drop, the simulated results indicate a good agreement with both the empirical model (Davies' model [35]) and the theoretical model

(Happel's model [33]). Additionally, the validation of filtration efficiency showed slightly over-prediction for the submicron particles and under-prediction of larger particles. However, the simulation was still able to follow the trend and provide the prediction within the variability of the experimental data [20]. The findings from this study revealed significant variations in filtration efficiency among different weave patterns, namely plain, satin, and twill weaves. The results consistently demonstrated that the satin weave exhibited the highest filtration efficiency, followed by the twill weave, while the plain weave consistently performed the least effectively across all tested velocities. The study additionally illustrated the impact of particle size on filtration efficiency. For example, Brownian diffusion was a dominant mechanism for smaller particles, resulting in similar filtering efficiency across all weave designs at the particle size of  $\leq 10$  nm. In addition, as the particle size increased (i.e., 0.01 – 10  $\mu\text{m}$ ), the impact of the weave pattern became more evident. The influence of inertial and interception mechanisms became more dominant as the particle size was further increased. Consequently, the filtration efficiency was increased with the particle size and flow velocity. The research gives useful information for enhancing filtration in woven filter cloths for workout masks. Weave patterns are important in obtaining improved filtering effectiveness, especially for the particles within the size range of 0.01 – 10  $\mu\text{m}$ . Furthermore, this study adds to our understanding of the effects of weave patterns on filtration effectiveness of fabric masks. Satin and twill weaves surpass plain weaves in terms of filtration efficiency at 0.05 m/s and 0.27 m/s. The latter represents the flow velocity for moderate exertion. Thus, the results can be applied for exercise-oriented fabric masks. Finally, for the simplification of the simulation, some influences such as reflection, elastic collisions of particles, humidity, particle shape, and micro-structure details of filter materials have been excluded. However, for a more comprehensive investigation, it is crucial to extend the study to consider these factors. Additionally, the formation of dendritic structures during filter operation highlights the importance of exploring the dynamics of particle deposition and its interplay with various parameters, contributing to a more integrated understanding of cloth filtration processes.

### Acknowledgement

This research was supported by the Second Century Fund Chulalongkorn University (C2F).

### References

- [1] World Health Organization. "Ambient Air Pollution: Health Impacts." Accessed: March 29, 2023. [Online]. Available: [https://www.who.int/news-room/fact-sheets/detail/ambient-\(outdoor\)-air-quality-and-health](https://www.who.int/news-room/fact-sheets/detail/ambient-(outdoor)-air-quality-and-health)

- [2] X. Yang, T. Zhang, X. Zhang, C. Chu, and S. Sang, "Global burden of lung cancer attributable to ambient fine particulate matter pollution in 204 countries and territories, 1990–2019," *Environ. Res.*, vol. 204, pp. 112023, 2022.
- [3] World Health Organization. "Transmission of SARS-CoV-2: implications for infection prevention precautions." Accessed: March 29, 2023. [Online]. Available: <https://www.who.int/news-room/commentaries/detail/transmission-of-sars-cov-2-implications-for-infection-prevention-precautions>
- [4] K. L. Andrejko, J. M. Pry, J. F. Myers, N. Fukui, J. L. DeGuzman, J. Openshaw, J. P. Watt, J. A. Lewnaed, and S. Jain, "Effectiveness of face mask or respirator use in indoor public settings for prevention of SARS-CoV-2 infection," *MMWR Morb Mortal Wkly Rep.*, vol. 71, no. 6, pp. 212-216, 2022.
- [5] N. Jones, J. Oke, S. Marsh, K. Nikbin, J. Bowley, H. P. Dijkstra, F. D. R. Hobbs, and T. Greenhalgh, "Face masks while exercising trial (MERIT): A cross-over randomised controlled study," *BMJ.*, vol. 13, no. 1, p. e063014, 2023.
- [6] S. Rengasamy, R. Shaffer, B. Williams, and S. Smit, "A comparison of facemask and respirator filtration test methods," *J. Occup. Environ. Hyg.*, vol. 14, no. 2, pp. 92-103, 2017.
- [7] V. Stadnytskyi, P. Anfinrud, and A. Bax, "Breathing, speaking, coughing or sneezing: What drives transmission of SARS-CoV-2?" *J. Intern. Med.*, vol. 290, no. 6, pp. 1010-1027, 2021.
- [8] K.-L. Tung, J.-S. Shiau, C. J. Chuang, Y. L. Li, and W.-M. Lu, "CFD analysis on fluid flow through multifilament woven filter cloths," *J. Sep. Sci.*, vol. 37, no. 4, pp. 799-821, 2002.
- [9] S. I. Green, Z. Wang, T. Waung, and A. Vakil, "Simulation of the flow through woven fabrics," *Comput Fluids.*, vol. 37, no. 9, pp. 1148-1156, 2008.
- [10] S. Q. Li, and J. S. Marshall, "Discrete element simulation of micro-particle deposition on a cylindrical fiber in an array," *J. Aerosol Sci.*, vol. 38, no. 10, pp. 1031-1046, 2007.
- [11] F. Qian, N. Huang, X. Zhu, and J. Lu, "Numerical study of the gas-solid flow characteristic of fibrous media based on SEM using CFD-DEM," *Powder Technol.*, vol. 249, pp. 63-70, 2013.
- [12] L. Zhang, J. Zhou, B. Zhang, and W. Gong, "Semi-analytical and computational investigation of different fibrous structures affecting the performance of fibrous media," *Sci. Prog.*, vol. 103, no. 1, 2020.
- [13] S. Han, J. Kim, and S. H. Ko, "Advances in air filtration technologies: Structure-based and interaction-based approaches," *Mater. Today Adv.*, vol. 9, p. 100134, 2021.
- [14] M. Zhu, J. Han, F. Wang, W. Shao, R. Xiong, Q. Zhang, H. Pan, Y. Yang, S. K. Samal, F. Zhang, and C. Huang, "Electrospun nanofibers membranes for effective air filtration," *Macromol Mater Eng.*, vol. 302, no. 1, p. 1600353, 2017.
- [15] A. B. Wang, X. Zhang, L. J. Gao, T. Zhang, H. J. Xu, and Y. J. Bi, "A review of filtration performance of protective masks," *J. Environ. Health*, vol. 20, no. 2346, 2023.
- [16] M. S. A. Heikkinen and N.H. Harley, "Experimental investigation of sintered porous metal filters," *J. Aerosol Sci.*, vol. 31, pp. 721-738, 2000.
- [17] K. W. Lee and B. Y. H. Liu, "On the minimum efficiency and the most penetrating particle size for fibrous filters," *J. Air Waste Manag. Assoc.*, vol. 30, no. 4, pp. 377-381, 1980.
- [18] F. T. Peirce, "Geometry of cloth structure," *Textile Research Journal*, vol. 28, pp. 45-96, 1937.
- [19] Y. Liu, L. Liu, Z. Li, Y. Zhao, J. Liu, and J. Yao, "3D network structure and sensing performance of woven fabric as promising flexible strain sensor," *SN Appl. Sci.*, vol. 2, pp. 1-13, 2020.
- [20] A. Konda, A. Prakash, G. A. Moss, M. Schmoldt, G. D. Grant, and S. Guha, "Aerosol filtration efficiency of common fabrics used in respiratory cloth masks," *ACS Nano*, vol. 14, no. 5, pp. 6339-6347, 2020.
- [21] S. A. Hosseini, and H. V. Tafreshi, "3-D simulation of particle filtration in electrospun nanofibrous filters," *Powder Technol.*, vol. 201, no. 2, pp. 153-160, 2010.
- [22] N. M. Zahari, M. H. Zawawi, L. M. Sidek, D. Mohamad, Z. Itam, M. Z. Ramli, A. Syamsir, A. Abas, and M. Rashid, "Introduction of discrete phase model (DPM) in fluid flow: A review," *AIP Conference Proceedings*, vol. 2030, p. 020234, 2018.
- [23] M. Mezhericher, T. Brosh, and A. Levy, "Modeling of particle pneumatic conveying using DEM and DPM methods," *Part. Sci. Technol.*, vol. 29, no. 2, pp. 197-208, 2011.
- [24] K. W. Chu, B. Wang, and A. Yu, "Discrete particle simulation of the gas-solid flow in a Circulating Fluidized Bed," in *The 12th International Conference on Fluidization - New Horizons in Fluidization Engineering*, Vancouver, Canada, 2007.
- [25] M. Dong, J. Li, Y. Shang, and S. Li, "Numerical investigation on deposition process of submicron particles in collision with a single cylindrical fiber," *J. Aerosol Sci.*, vol. 129, pp. 1-15, 2019.
- [26] P. G. Saffman, "The lift on a small sphere in a slow shear flow," *Journal of Fluid Mechanics*, vol. 22, no. 2, pp. 385-400, 1965
- [27] B. Cao, S. Wang, W. Dong, J. Zhu, F. Qian, J. Lu, and Y. Han, "Investigation of the filtration performance for fibrous media: Coupling of a semi-analytical model with CFD on Voronoi-based microstructure," *Sep. Purif. Technol.*, vol. 251, p. 117364, 2020.
- [28] Y. Zhu, W. C. Hinds, S. Kim, and C. Sioutas, "Concentration and size distribution of ultrafine particles near a major highway," *J. Air Waste Manag. Assoc.*, vol. 52, no. 9, pp. 1032-1042, 2002.

- [29] F. Qian, N. Huang, J. Lu, and Y. Han, "CFD–DEM simulation of the filtration performance for fibrous media based on the mimic structure," *Comput. Chem. Eng.*, vol. 71, pp. 478-488, 2014.
- [30] I. Rios de Anda, J. W. Wilkins, J. F. Robinson, C.P. Royall, and R.P. Sear, "Modeling the filtration efficiency of a woven fabric: The role of multiple lengthscales," *Phys. Fluids*, vol. 34, no. 3, p. 033301, 2022.
- [31] C. C. Coffey, C. L. Campbell, and Z. Zhuang, "Simulated workplace performance of N95 respirators," *Am. Ind. Hyg. Assoc. J.*, vol. 60, no. 5, pp. 618-624, 1999.
- [32] W. C. Hinds, *Aerosol Technology: Properties, Behaviour and Measurement of Airborne Particles*. Wiley, 1999.
- [33] J. Happel, "Viscous flow relative to arrays of cylinders," *AICHE Journal*, vol. 5, no. 2, pp. 174-177, 1959.
- [34] S. Kuwabara, "The forces experienced by randomly distributed parallel circular cylinders or spheres in a viscous flow at small Reynolds numbers," *J. Phys. Soc. Japan.*, vol. 14, no. 4, pp. 527-532, 1959.
- [35] C. N. Davies, *Air Filtration*. Academic Press, 1973.
- [36] N. Rao and M. Faghri, "Computer modeling of aerosol filtration by fibrous filters," *J. Aerosol Sci.*, vol. 8, no. 2, pp. 133-156, 1988.
- [37] H. Bai, X. Qian, J. Fan, Y. Shi, Y. Duo, C. Guo, and X. Wang, "Theoretical model of single fiber efficiency and the effect of microstructure on fibrous filtration performance: A review," *Ind. Eng. Chem. Res.*, vol. 60, no. 1, pp. 3-36, 2021.
- [38] D.-L. Liu, "Particle deposition onto enclosure surfaces," in *Developments in Surface Contamination and Cleaning*, R. Kohli and K. L. Mittal, Eds. William Andrew Publishing, 2010, ch. 1, pp. 1-56.



**Wisit Bandasak**, photograph and biography not available at the time of publication.

**Pimporn Ponpesh**, photograph and biography not available at the time of publication.